



# Low flow, high head

---

**Internship assignment**  
**Flowserve flow solutions group**

---

Remco Olimulder  
Master student Mechanical Engineering,  
Chair Engineering Fluid Dynamics

**UNIVERSITEIT TWENTE.**



# Internship report

This is a report of the internship I carried out at Flowserve Hengelo. The internship is part of the curriculum of the master Mechanical Engineering at the University of Twente.

Carried out by:	Remco Olimulder S0185132
Host institution:	Flowserve hengelo Hengelo, the Netherlands
Supervisor host institution:	Niels Platenkamp
Home institution:	University of Twente Enschede, the Netherlands
Supervisor home institution:	Prof. Dr. Ir. C.H. Venner
Duration of the internship:	September 22nd 2014 - December 19th 2014



# Management Summary

In the petrochemical industry, centrifugal pumps are extensively used in a wide range of applications. The pump characteristics, such as required head and flow rate, can be specified using the pump specific speed. Of particular design interest to Flowserve Hengelo are the pumps with low specific speeds. These are pumps with a high head and low flow rate. In these pumps hydraulic and secondary losses play a larger role. Also pumps tend to become unstable at flow rates below the design flow rate, thus diminishing the stable operating range. Because customers require a continuous rising head-flow rate curve from the design point to the shut-off point, some research shall be done to better understand the flow phenomenon occurring at part load and to implement this in a design strategy. The first part of this report is a literature study to find out what is already known about the flow through a centrifugal diffuser pump at part load. Also some research was done to find possible solutions to increase the stable operating range of low specific speed centrifugal diffuser pumps. Since the head loss at part load seems to be caused by the diffuser geometry, this research concentrates on different diffuser geometries. Little was found on centrifugal diffuser pumps, however, expanding the search to include centrifugal compressors did result in some solutions. The second part of this report deals with the implementation of the proposed solutions in computational models to test their effect on the stability, head capacity curve and efficiency of the pump. The third part will be to actually produce the designed diffusers and test them with the specified impeller. And of course relate the test results to the CFD results. The final step can be to optimize the design procedure for centrifugal diffuser pumps with low specific speeds.



# Contents

<b>Contents</b>	<b>v</b>
<b>List of Figures</b>	<b>vii</b>
<b>1 introduction</b>	<b>1</b>
1.1 Flowserve [1]	1
1.2 radial diffuser pumps	1
1.3 outline	1
<b>2 Literature study</b>	<b>3</b>
2.1 flow phenomena	3
2.1.1 impeller-diffuser interaction	4
2.1.2 flow phenomena in the diffuser	6
2.2 improving head under part load conditions	7
2.2.1 clearance	7
2.2.2 hooked or tapered vanes	8
2.2.3 vane grooves	10
2.2.4 hub and shroud grooves	14
2.3 Numerical and practical test plan	15
<b>3 numerical simulation</b>	<b>17</b>
3.1 Reference impeller calculations	17
3.2 diffuser calculations	18
3.2.1 variation of number of diffuser blades	19
3.2.2 Varying boundary conditions	20
3.2.3 conclusion	26
3.3 Nonlinear hydraulic calculations	26
3.3.1 diffuser model	26
3.3.2 FINE/Turbo settings	27
3.3.3 results	28
<b>4 testing</b>	<b>31</b>
4.1 test stand	32
4.2 test results	32
<b>Bibliography</b>	<b>35</b>



# List of Figures

2.1	mid height velocity fields in the impeller for the design flow rate [3] . . . .	4
2.2	numbering of the impeller channels [3] . . . . .	5
2.3	Impeller exit velocity fields [3] . . . . .	5
2.4	Diffuser mid-height velocity and vorticity fields [4] . . . . .	6
2.5	performance for different single sided clearance sizes [5] . . . . .	7
2.6	performance for different two sided clearance sizes [5] . . . . .	8
2.7	hooked diffuser vanes . . . . .	9
2.8	tapered diffuser vanes . . . . .	9
2.9	performance for different taper designs [5] . . . . .	10
2.10	performance for hub or shroud taper[9] . . . . .	10
2.11	grooves in the diffuser vane . . . . .	11
2.12	head capacity curve, D=1.5, L=0.23 . . . . .	11
2.13	head capacity curve; D=1.5, L=0.29 . . . . .	12
2.14	head capacity curve; D=1.22, L=0.29 . . . . .	12
2.15	Comparison of the test results . . . . .	13
2.16	design of the diffuser grooves[13] . . . . .	14
2.17	tangential and radial velocity for a diffuser[13] . . . . .	14
3.1	Free impeller calculations . . . . .	18
3.2	Diffuser pressure loss and impeller-diffuser combined head . . . . .	19
3.3	figures from[16] . . . . .	21
3.4	inlet and outlet mass flow convergence . . . . .	24
3.5	velocity field at mid plane . . . . .	24
3.6	Inlet radial velocity distribution . . . . .	25
3.7	inlet tangential velocity distribution . . . . .	25
3.8	unstructured block grid . . . . .	27
3.9	structured block grid . . . . .	27
3.10	Pump head coefficient vs time steps . . . . .	29
3.11	complete pump characteristics . . . . .	29
3.12	Diffuser and impeller characteristics . . . . .	30
4.1	CAD images of the tested diffusers . . . . .	31
4.2	test pump . . . . .	32
4.3	head coefficient - flow coefficient and relative efficiency - flow coefficient curves for the tested designs . . . . .	33
4.4	Measured shaft displacement . . . . .	34



# 1 introduction

## 1.1 Flowserve [1]

Flowserve is a world leader in supplying pumps, valves, seals and related services. The main markets are oil and gas, chemical and pharmaceutical industry, power generation and water. It was founded in 1997 with a merger between BW/IP and Durco International. In the same year they acquired Stork engineered pumps, the current Flowserve Hengelo division. It grew larger through mergers and acquisitions and now has over 15000 employees in over 50 countries, making it the second largest pump manufacturer in the world.

### Flowserve Hengelo

The Hengelo division of Flowserve, the former Stork pompen, has specialized in centrifugal pumps for 2 main markets. These are the water market, consisting mostly of cooling water, irrigation and drainage pumps, and the process market, consisting of pumps for the chemical, oil and gas industry. For the process market, most pumps are of the radial diffuser type.

## 1.2 radial diffuser pumps

The most important parts of a radial diffuser pump are the impeller with axial inflow and radial outflow and a diffuser ring decelerating the flow after it leaves the impeller. Lately, research is being done to improve single stage pumps capable of pumping low flow rates up to high pump heads. However one of the problems encountered in this process is the fact that these small pumps don't have a stable head-capacity curve. Research has indicated that this is probably caused by the diffuser.

## 1.3 outline

The aim of this internship is to study the effect of different diffuser geometries on the head generated by a pump for different flow rates. In chapter 2 a review of pump theory is given for design and off design flow. Also research was done to find some solutions already being applied to increase pump efficiency and head at off design conditions. In chapter 3 the numerical simulation procedure is given. Also some problems encountered during simulating are discussed as well as how they were solved. The final chapter, chapter 4 shall deal with the physical testing. The test stand shall be explained and results and conclusions are presented.



## 2 Literature study

The first part of the internship was to learn what happens inside a centrifugal diffuser pump, both during normal operation and, of particular interest, during part load operation. To this end, section 2.1 describes what happens inside a centrifugal diffuser pump, more specific for the region between the impeller and diffuser, and inside the diffuser. Section 2.2 deals with the literature found on ways to improve the head generated by a pump under part-load conditions. Literature found on this topic is discussed here as well as some prior research results already found by Flowserve Hengelo. The final section, section 2.3, shortly describes the plans for the simulation and physical test part of the internship.

### 2.1 flow phenomena

A centrifugal diffuser pump consists of a radial impeller with or without a shroud surface, inside a pump casing. Surrounding the radial impeller is a stationary radial diffuser consisting of a vaneless space, or several vanes directing the flow and slowing it down in order to increase the static pressure at the exit of the pump casing. In a vaneless diffuser, the fluid has a large area over which the velocity builds off and the static pressure increases. Typically, this type of diffuser has a stable but relative flat flow rate - head curve. A vaned diffuser is more widely used in industrial applications because it has higher pressure increase and a steeper flow rate - head curve. One of the drawbacks of a vaned diffuser however, is the smaller stable range of operation. This is due to the vane angle, which is optimal for the design point, but invokes incidence losses at part load, up to the part where boundary layer separation occurs and the diffuser stalls. This leads to a drop in generated head and thus introduces an instability. The main focus of this report is to find possible causes for the boundary layer separation and possible solutions to delay the onset of stall to lower flow rates.

At the design flow rate, the fluid leaves the impeller at a certain flow angle, based on the rotational speed of the impeller and the flow rate through the pump. This flow angle is the design incidence angle for the vanes of the diffuser. This means that the fluid leaving the pump is flowing exactly in the direction that the leading edge of the vane is pointed. If the flow rate through the pump is diminished, for example by partially or completely closing a valve in the exit pipe, the pump is said to operate at part load condition. The effect of this is that the impeller exit flow angle shifts towards more tangential flow, because of the lower radial velocity of the fluid. Since the diffuser angle is fixed, this leads to diffuser incidence losses and lower flow through the diffuser. This however is in theory, and based on the time averaged flow.

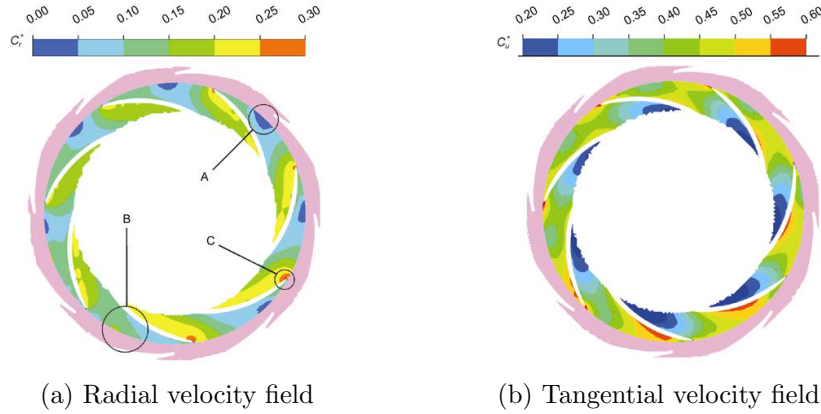


Figure 2.1: mid height velocity fields in the impeller for the design flow rate [3]

### 2.1.1 impeller-diffuser interaction

In practice, there is interaction between the impeller trailing edge and the leading edge of the diffuser vanes because of the high velocity difference and relatively small radial distance between them. *Atif A, Benmansour S, Bois G, et al.* [3] simulated this interaction using a frozen rotor CFD model, and verified their results using PIV measurements. The effect of impeller-diffuser interaction on the flow field at mid height can be seen in figure 2.1.

In figure 2.1a it can be seen that a region of low radial velocity forms in each channel of the impeller, just upstream of the diffuser leading edge. The size of this region depends on the position of the leading edge of the diffuser relative to the positions of the blades of the impeller; the farther away from the blades of the impeller, the larger the region. Also a region of high radial velocity forms on the pressure side trailing edge of the impeller blades from the moment it has passed the diffuser vane leading edge. This region grows in size and progresses up to the leading edge of the impeller blade over the course of passing 1 diffuser channel. It breaks when the trailing edge of the impeller vane and leading edge of the diffuser vane are closest together. In figure 2.1b it can be seen that for the tangential velocity something similar happens. On the suction side leading edge a region of large tangential velocity is formed radially inward from the diffuser vane leading edge. Over the course of passing 1 diffuser channel, the magnitude of tangential velocity increases and the region progresses to the trailing edge of the impeller vane.

In the previous section, the velocity field at mid height was considered. However, a variation in velocity field can also be found when going from the hub to the shroud of the impeller. When looking at the velocity field from hub to shroud, the impeller channels need to be numbered to distinguish the different channels. Thus a numbering was made as in figure 2.2, and radial and tangential velocity fields were visualized for the different impeller channels. Figure 2.3 shows the radial and tangential velocity fields between hub and shroud, from pressure to suction side of the impeller channel for 3

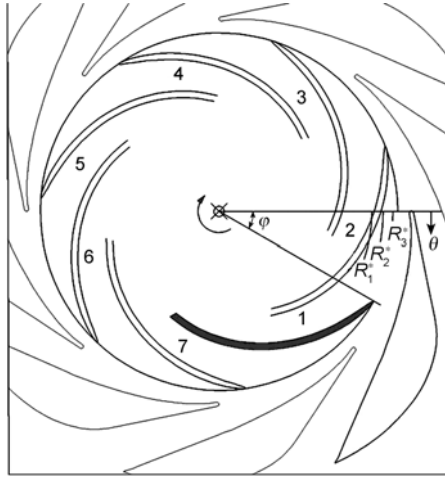


Figure 2.2: numbering of the impeller channels [3]

different channels. In channel 1, the diffuser vane leading edge is near the suction side of the impeller; in channel 3, it is in the middle of the impeller channel and in channel 6, the diffuser vane leading edge is near the pressure side of the impeller. So over one rotation first the situation in channel 6 is observed, then the situation of channel 3 and finally that of channel 1. When looking at the radial velocity field, it can be seen that the region of low radial velocity concentrates around the meridional plane. Near the hub and the shroud there is a more constant radial velocity. Also, the region of high radial velocity starts to form on the hub and shroud of the impeller and spreads over the whole width of the impeller as the impeller vane moves towards the diffuser vane.

When looking at the tangential velocity field, it can be seen that the tangential velocity is highest near the hub and shroud when the diffuser vane is on the trailing edge pressure side, and highest in the meridional plane when the diffuser vane is near the trailing edge suction side. When the diffuser vane leading edge is approximately in between 2 impeller blades, there is a region of low tangential velocity in the centre of the impeller with slightly higher tangential velocity on the hub and shroud.

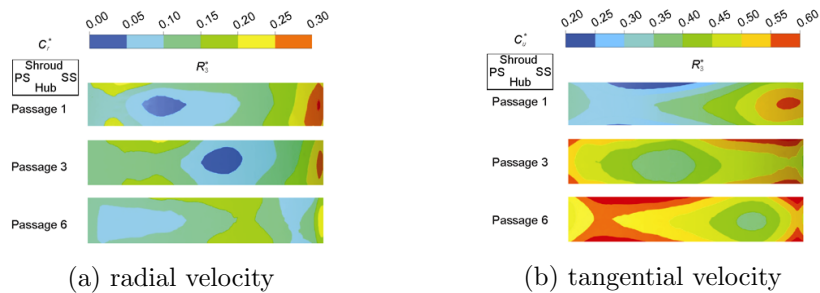


Figure 2.3: Impeller exit velocity fields [3]

## 2.1.2 flow phenomena in the diffuser

The interaction between impeller and diffuser causes the flowfield into the diffuser to fluctuate. *Gaetani P, Boccazzi A and Sala R* [4] used 2D particle image velocimetry to visualize the time averaged flow field and vorticity inside the diffuser of a centrifugal pump at design flow rate as well as under part-load conditions. When looking at the flow field in figure 2.4a and 2.4b, it can be seen that the magnitude of the velocity at inlet to the diffuser is approximately the same at the design flow rate and at part-load conditions. However, the velocity after the diffuser vanes is considerably lower under part-load conditions. Also the direction of the flow is more tangentially directed under part-load compared to the design flow rate. This corresponds with the design theory. It can be seen that the velocity field near the pressure side of the diffuser blades changes the most under part load, while the velocity field near the suction side is approximately the same. The same can be concluded for the vorticity field under design conditions and part-load conditions. Under part-load conditions there is a region of low flow and low vorticity which has its origin approximately halfway the blade. This is believed to be caused by flow separation due to the incorrect incidence angle of the diffuser blade.

Another important flow phenomenon was discovered by *Goto T, Ohmoto E, Ohta Y and Oota E*. [8]. They did CFD calculations and experiments on a centrifugal compressor with a vaneless and vaned diffuser. One of the results was the presence of a vortex on the leading edge of the diffuser vanes caused by a reverse flow on the shroud side of the leading edge. The scale of this leading edge vortex becomes larger with decreasing flow rate and blocks the stream into the diffuser passage. This could be one of the causes leading to diffuser stall and unstable head curves.

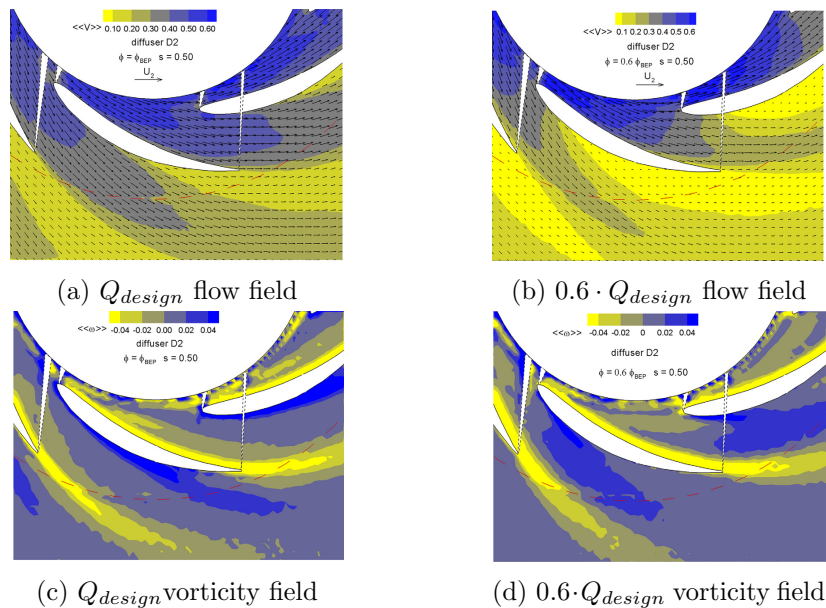


Figure 2.4: Diffuser mid-height velocity and vorticity fields [4]

## 2.2 improving head under part load conditions

In this section, several diffuser designs are presented and their effect on pump operations under part-load shall be discussed. Several papers on this topic were presented by *Ohta Y et al.*[5, 6, 7, 8, 9], suggesting a few different designs. However, the tests were run with a centrifugal compressor, and the main objective was to reduce noise and maintain or improve the pressure recovery around BEP.

Another possible solution is already being used at Flowserve. In the past, Flowserve engineers have had some positive results improving the head flow rate curve by adding a groove to the vane surface just upstream of the throat. No literature was found explaining this specific solution but some of the test results shall be discussed. Besides this, there was some literature on radial grooves in the hub and/or shroud casing improving performance under low flow conditions.

### 2.2.1 clearance

The first improvement proposed by *Ohta Y et al.*[5] was to create a clearance between the diffuser vanes and the hub or shroud of the diffuser, or on both sides of the diffuser vanes. They found that a clearance of 5% or 10% on either the hub or the shroud showed the best results, giving a smaller flow separation region behind the leading edge. However, using only a hub- or shroud side clearance resulted in deterioration of the pressure recovery, as can be seen in figure 2.5, and generated a non-uniform flow field in the diffuser. In order to cancel this non-uniform flow field, a 2-sided clearance was tested.

For the two sided clearance, tests were run for a symmetrical clearance of 5% and 10%

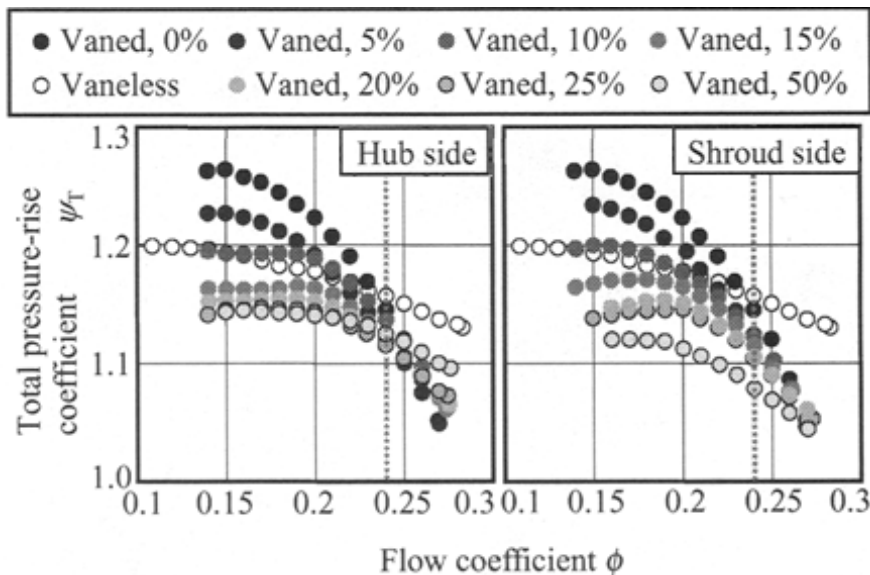


Figure 2.5: performance for different single sided clearance sizes [5]

on both sides as well as for a asymmetrical clearance consisting of 5% hub side and 15% shroud side clearance or vice versa. The asymmetrical case showed little improvement over the single sided clearance, possibly due to the non-uniform flow field still existing in the diffuser. However, the symmetrical case did show performance improvement over the single sided clearance. Especially in the low flow regime, the pressure recovery is improved. Also the onset of instability isn't detected in the tested flow range. Compared to the normal vaned diffuser however, there is still a performance decrease over the complete range of flow rates. This can be seen in picture 2.6

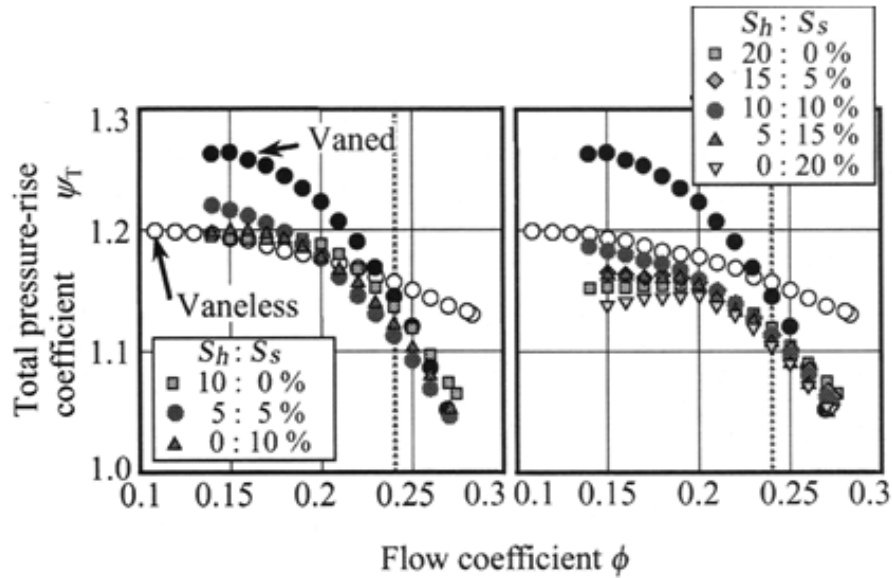
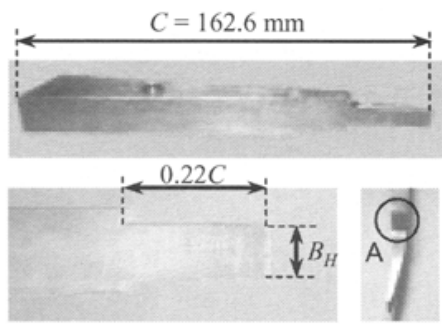


Figure 2.6: performance for different two sided clearance sizes [5]

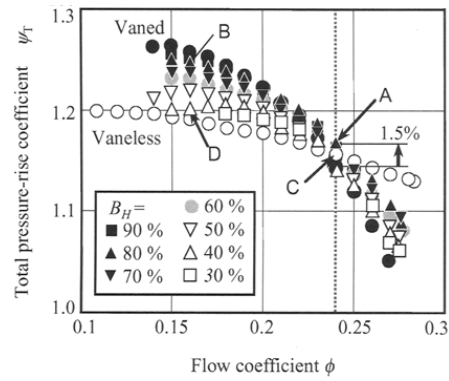
### 2.2.2 hooked or tapered vanes

*Ohta Y et al.* figured the performance decrement is caused by the secondary flow in the vaneless space which consists of rotating flow and leakage flow due to the clearance on both sides of the diffuser vanes. In order to suppress the performance decrease caused by the rotating flow, the hooked diffuser vane shown in figure 2.7a was developed. There is a two sided clearance from the leading edge up to 22% chord length. This hooked vane was tested with a leading edge width  $B_H$  of 90% to 30%, results are shown in figure 2.7b. It can be seen that a leading edge width of 70% to 90% gives best performance in low flow regime as well as improved performance at BEP. Onset of instability is also delayed to a lower flowrate compared to the vaned diffuser so the hooked vane has some potential of improving the pump operation range.

As a follow up to the hooked vane, a tapered vane was proposed to reduce the effect of the corner of the hook on the flow field and induced losses in the diffuser. Three designs were tested, A) from the leading edge to 22% chord; B) from the leading edge to 30% chord; C) 3D tapered, with different taper lengths on pressure and suction side.

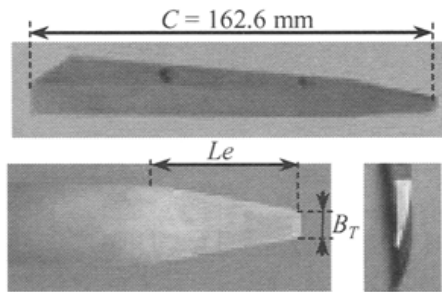


(a) Hooked diffuser vane design [5]



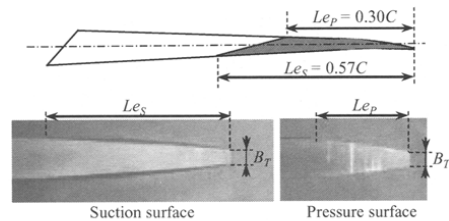
(b) performance of different vanes [5]

Figure 2.7: hooked diffuser vanes



Type A :  $Le = 0.22C$ , Type B :  $Le = 0.30C$

(a) 2D [5]



(b) 3D tapered diffuser vane type C

(b) 3D [5]

Figure 2.8: tapered diffuser vanes

Different leading edge heights from  $B_T=30\%$  to  $B_T=90\%$  were tested. Since the scope of their research was to improve efficiency at BEP as well as reduce operation noise, they found the tapered vane with  $B_T=40\%$  to be the best and only displayed this result. Comparing this result to the case of the hooked diffuser vane, the expectation is that a leading edge height of 60% to 80% will result in better low flow rate operation and possibly extended operating range. 2 other tests were run testing 3D tapered diffuser vanes with different geometries [6, 7] showing the same result. The next research done by *Ohta et al*[9] was aimed at improving low flow operation of a centrifugal compressor. Because the deterioration in performance is probably caused by a leading edge vortex, single side tapered diffuser vanes were tested, with a taper on the hub or shroud side only. This was tested numerically only, it wasn't evaluated using experimental procedures like PIV or LDV. The result however showed that a diffuser vane with a 3D tapered part on the hub side only has the potential to improve performance in the low flow rate range, and to extend the operating range to lower flow rates.

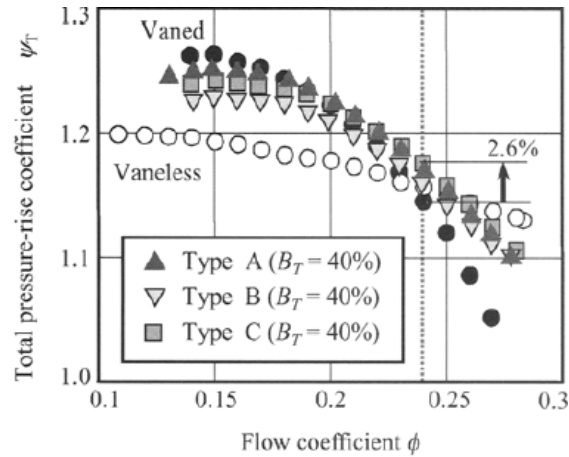


Figure 2.9: performance for different taper designs [5]

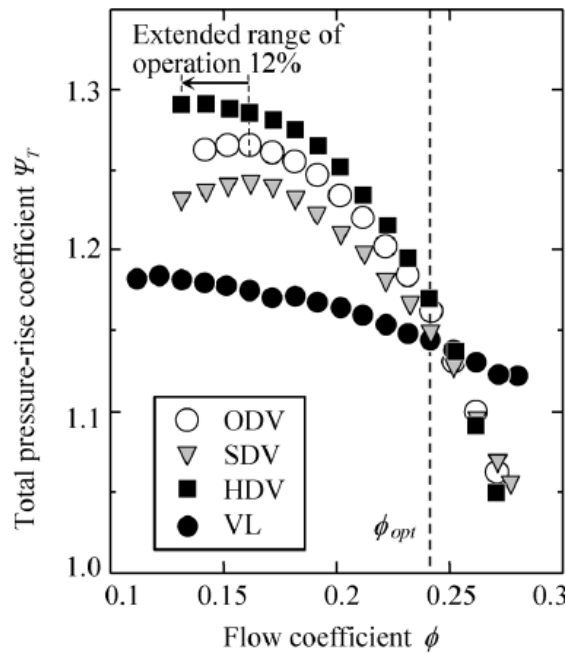


Figure 2.10: performance for hub or shroud taper[9]

### 2.2.3 vane grooves

For several different radial diffuser pumps, with different mass flow rates and diameters, Flowserve had already encountered the problem of drooping head-capacity curves. Experience learned that adding a small groove in the triangular vaneless space in front of the throat area could solve this and give a more stably rising head-capacity curve. In three cases the changes made to the diffuser were documented and several different groove depths were tested.

The first record was of an 8 bladed diffuser with an unstable head-capacity curve. The pump had a specific speed of  $N_s = 0.32$ . It was decided to machine a groove into the diffuser consisting of a circular section with a radius of 1 mm, starting perpendicular to the vane surface, and a straight section connecting the end of the circular section with the vane surface. The length of the groove was kept constant at 0.23 times the length AB in figure 2.11. The start of the groove is positioned at a relative distance of 1.5. The relative distance is defined as the distance of the groove to the trailing edge divided by the diffusion length to the trailing edge, where the diffusion length is the length of the diffusion channel running from C to B in figure 2.11.

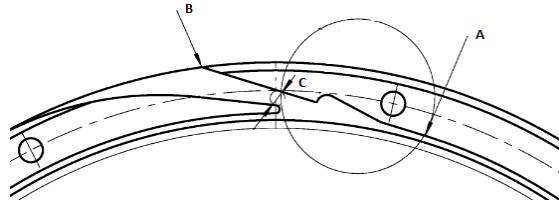


Figure 2.11: grooves in the diffuser vane

The effect of this groove was an overall rise of the head-capacity curve with approximately 1.5%. However, the curve was still unstable and the head rise to shutoff slightly decreased. The next step was to increase the groove depth to 3 mm. This resulted in a stably rising head-capacity curve with lower rated head and slightly higher shutoff head. The 3 head-capacity curves can be seen in figure 2.12. The head is made dimensionless by dividing with the rated head at BEP. The flow rate is made dimensionless by dividing with the flow rate at BEP.

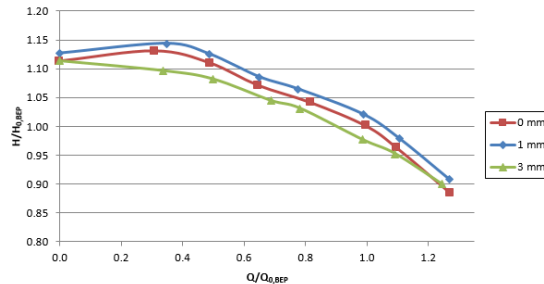


Figure 2.12: head capacity curve,  $D=1.5$ ,  $L=0.23$

The next recorded use of a groove is in a pump with a 3 bladed diffuser, also with a drooping head-capacity curve. This pump had a specific speed of  $N_s = 0.07$ . Since this pump has a much lower specific speed it was decided to run a second series of tests. Again the groove was placed at a relative distance of 1.5. The groove length was changed to approximately 0.29 times length AB. The first test had a groove depth of 2 mm. This resulted in a slightly lowered rated head and a little increase in the shutoff head. Increasing the groove through 3 mm to 4 mm increased the rated head and gave a

head-capacity curve with just a slight instability at shutoff. Increasing the groove depth even further to 5 mm resulted in a curve comparable to that of the 4 mm groove, but shifted towards lower head. This can be seen in figure 2.13.

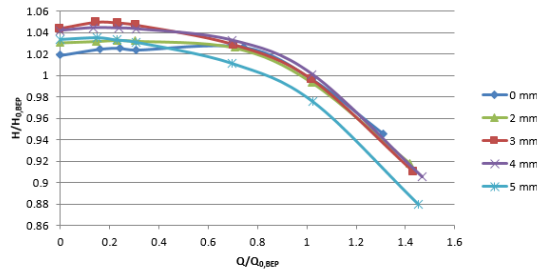


Figure 2.13: head capacity curve;  $D=1.5$ ,  $L=0.29$

In a subsequent test with a comparable pump, one with a specific speed of  $N_s = 0.08$  the head-capacity curve was stable, however, the head rise to shutoff was too low. In other words, the difference between the rated head and shutoff head was too small. So a groove was machined in the diffuser with a depth of 3 mm and length of approximately 0.29 times the length AB. This time the relative distance was changed to 1.22. This increased the head rise to shutoff, but also introduced an instability below 25% of the rated flow. The head-capacity curve can be seen in figure 2.14.

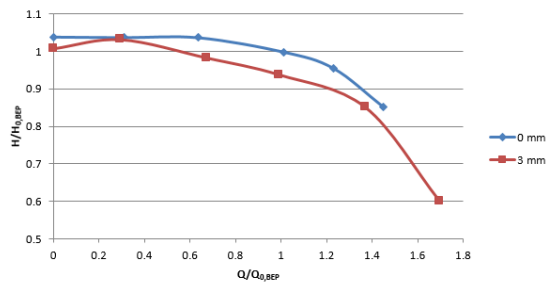


Figure 2.14: head capacity curve;  $D=1.22$ ,  $L=0.29$

## conclusions

To compare the results of the different tests, we use the relative head rise, the relative shut-off head rise and the rise in head rise to shut-off, as defined in equations (2.1-2.3)

$$\text{Relative head rise} : \frac{H_{groove,rated} - H_{original,rated}}{H_{original,rated}} \quad (2.1)$$

$$\text{Relative shut-off head rise} : \frac{H_{groove,shut-off} - H_{original,shut-off}}{H_{original,shut-off}} \quad (2.2)$$

$$\text{Relative rise in head rise to shut-off} : \frac{\frac{H_{shut-off,groove}}{H_{rated,groove}} - \frac{H_{shut-off,original}}{H_{rated,original}}}{\frac{H_{shut-off,original}}{H_{rated,original}}} \quad (2.3)$$

The calculated relative values can be plotted with the groove depth on the horizontal axis, and one of the relative values on the vertical axis. That way the results of the three tests for the same relative value can be plotted in the same graph, as in figure 2.15. First for the effect of groove depth on the relative head rise at the rated capacity, it can be concluded that shallow grooves might improve the rated head. However, depending on the position and length of the groove, there is a certain depth after which the groove acts as a flow disturbance and as such lowers the generated head at rated flow. When looking at the shut-off head, it can be seen that the same thing is happening. Shallow grooves improve the shut-off head compared to the situation without grooves, but beyond a certain groove depth the shut-off head will decrease again and the groove starts acting more and more as an obstruction to the flow. Comparing the three different graphs, the grooves with a relative distance of 1.5 show approximately the same response to groove depth, though with a scaling factor. The groove with a relative distance of 1.22 generates a straight line, but this is due to the fact that there are only 2 measurements. When looking at the relative head rise to shut-off it can be seen to improve with the groove depth. Based on these results optimum groove parameters could be selected based on the specific needs per project. However, more data is needed to better predict the optimum parameters.

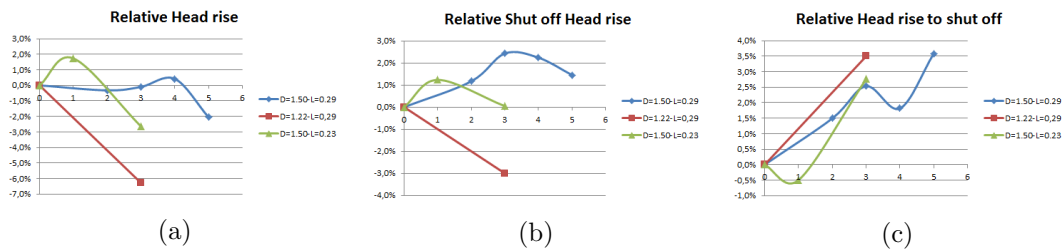


Figure 2.15: Comparison of the test results, groove depth on the horizontal axis

## 2.2.4 hub and shroud grooves

*Kurokawa et al.*[13, 14] experimented with a vaned diffuser in which the hub and shroud were machined to a certain depth and rubber plates were placed to create grooves, as can be seen in figure 2.16. This way the length, width and depth of the grooves could be varied. They concluded that rotating stall in a vaned diffuser can be suppressed completely using radial grooves. This is caused by the grooves reducing the tangential velocity, as can be seen in figure 2.17. As a side-effect however, the efficiency also decreases. Because a testplan was already set-up prior to finding this article, the effect of this diffuser modification hasn't been tested. This can be subject of further study towards improving radial diffuser pumps.

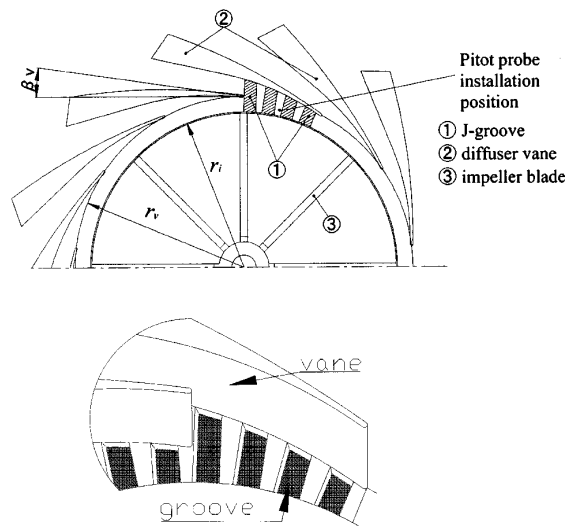


Figure 2.16: design of the diffuser grooves[13]

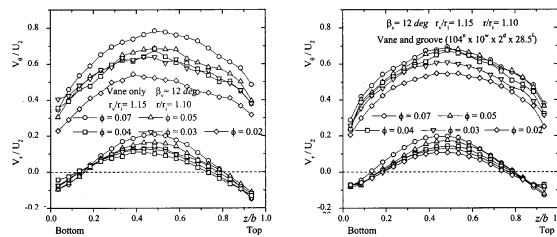


Figure 2.17: tangential and radial velocity for a diffuser with(right) or without grooves[13]

## 2.3 Numerical and practical test plan

After the literature study a brain storm session took place with Niels Platenkamp, Ronald Dijkers, Berry Kolkman, Lars Krakkers and myself discussing possibilities of improving diffuser design for low flow high head operating conditions. Based on their knowledge and experience and partially on the results found in literature, several proposals were thought of, and rated based on the likeliness of producing good results, the innovative character of the solution, technical difficulty and needed number of tests.

- **Reference test & simulations:** fitting a diffuser with 3, 4 or 5 blades, also a simulation was done with 20 thin aerofoil like blades.
- **groove:** a groove in the diffuser vane just before the start of the diffusion area, also a test was done with multiple successive grooves.
- **tapered vane:** A variation of the tapered vane shape found in literature.
- **diffuser in concentric pump casing** to test the effect of the pump casing on the diffuser efficiency.
- **axial outflow diffuser** a diffuser in which the diffuser channels only have outflow ports in axial direction. The idea behind this is that all radial and tangential velocity is converted, either to axial velocity or to static pressure thus improving the head curve.



## 3 numerical simulation

In this part, the numerical procedure shall be discussed. The program used for the numerical calculations is NUMECA Fine/Turbo V9.1. First, a free impeller calculation has been carried out for the test impeller. The used impeller is a 40-08-25-y8-40c impeller, or 40C for short. This impeller has 5 blades. The calculated mass flow and tangential velocity can be used as boundary conditions for free diffuser calculations. First, three diffusers were used for a reference calculation, testing the method. This way it was found that the diffusers suffer from large losses in the necessary inlet region, making it difficult to predict the right inlet boundary conditions as well as leading to unstable calculations at off design conditions. This led to a test of several different sets of inlet and outlet boundary conditions to get a solution set which approximates the results of physical tests. It was concluded that impeller diffuser interaction plays an important role so as a next step nonlinear hydraulic calculations of a complete model were carried out. For this a numerical model consisting of the rotor, diffuser and leakage paths was used which was previously used by Niels Platenkamp. Since the effect of varying the number of channels had already been tested on this model by Niels the effect of a groove in the diffuser was simulated and tested.

### 3.1 Reference impeller calculations

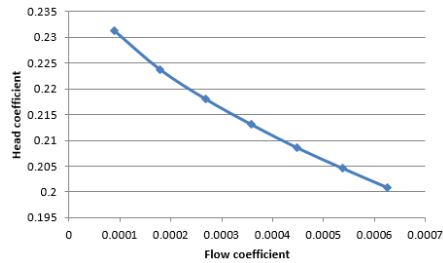
the aim of the numerical simulations is to run free diffuser calculations using a mass flow imposed boundary condition on the inlet to the diffuser. Therefore the tangential velocity at inlet to the diffuser is needed. This is a direct result of the flow out of the impeller for different flow rates. Thus first a free impeller calculation was done for the 40-08-25-y8 impeller. The first calculation was done for the test pump rotational speed of 1500 RPM, and design flow rate. A mass flow imposed boundary condition was specified on the inlet, while on the outlet an averaged static pressure imposed boundary condition was specified. The value of static pressure at outlet was estimated to be 1501.3 kPa. Numeca treats this pressure as a reference pressure and calculates the inlet pressure accordingly. As solid boundary condition it was chosen to impose an adiabatic, area defined rotation speed for the hub and the shroud, such that a non rotating inlet and outlet section exist, and an adiabatic constant rotation speed was imposed on the impeller blades. To check if the solution has converged to a stable solution, all quantities should have reached a stable value and residuals should be low.

Under these boundary conditions a set of simulations was run for  $Q = 20\%Q_{design}$  using steps of 20% up to  $Q = 140\%Q_{design}$ . The head coefficient and relative tangential velocity for the various flow rates can be found in table 3.1 and the head coefficient-flow

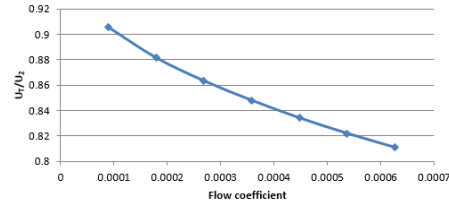
coefficient curve and relative tangential velocity-flow coefficient curve in figure 3.1. The head coefficient  $\Psi$  is given by:  $\Psi = \frac{gH}{N^2D^2}$ . The flow coefficient  $\Phi$  is given by:  $\Phi = \frac{Q}{ND^3}$ .

$\Phi$	$\Psi$	$U_T/U_2$
$8.94 \cdot 10^{-5}$	0.231	0.91
$1.79 \cdot 10^{-4}$	0.224	0.88
$2.68 \cdot 10^{-4}$	0.218	0.86
$3.58 \cdot 10^{-4}$	0.213	0.85
$4.47 \cdot 10^{-4}$	0.209	0.83
$5.37 \cdot 10^{-4}$	0.205	0.82
$6.26 \cdot 10^{-4}$	0.201	0.81

Table 3.1: Flow coefficient, head coefficient and relative tangential velocity for the 40C impeller



(a) head coefficient-flow coefficient curve



(b) relative tangential velocity - flow coefficient curve

Figure 3.1: Free impeller calculations

## 3.2 diffuser calculations

Now the performance curves of the impeller are known, as well as the tangential velocity at impeller exit for different flow rates. This tangential velocity, together with the mass flow rate, will serve as the inlet boundary condition for the diffuser calculations. The chosen inlet boundary condition is the mass flow imposed boundary condition for which the meridional flow angle and the tangential velocity are required. Since a radial diffuser is fitted to the pump, the meridional flow angle is purely radial. The tangential velocity that was found in section 3.1 was used. As a first test, simulations were run for a vane-island diffuser with 3, 4 and 5 blades and a constant AZ size. The results of these simulations were analyzed to check if the chosen settings give feasible results.

### 3.2.1 variation of number of diffuser blades

Using a python script file, the dynamic and static pressure at the inlet boundary and at the exit as well as the tangential velocity at the inlet boundary are printed. Using the difference in dynamic pressure between the inlet and outlet, the head loss through the diffuser can be calculated. The resulting head coefficient is plotted in figure 3.2a. When the impeller generated head and the head loss through the diffuser are combined, the total generated head is found. Again, the resulting head coefficient is shown in figure 3.2b.

It can be seen that the 3-bladed diffuser shows an increase in head loss below a certain flow rate, resulting in a drooping head-capacity curve. The head loss over the diffuser for the 4-bladed and 5-bladed diffuser keep decreasing, resulting in a continually rising head-capacity curve. Since this is in contradiction with test results, the diffuser inlet relative tangential velocities were plotted in figure 3.2c.

As can be seen, the relative tangential velocity at inlet to the diffuser increasingly deviates from the free impeller case with decreasing flow rate. Since this effect was expected, already an increasingly larger tangential velocity was imposed with decreasing flow rate. Because of the large deviation of the relative tangential velocity, a new simulation was run for the 5-bladed diffuser and a flow coefficient of  $\Phi = 0.64$ . A larger tangential velocity was imposed on the inlet boundary. The result of this calculation can also be found in figure 3.2. Although this still didn't satisfy the actual boundary condition at the diffuser inlet, it did show that the 5 bladed impeller also is unstable under low flow conditions, which can be seen by the single cross in figure 3.2a. Also, it was concluded that the losses in the inlet section increase with increasing tangential velocity as well as with decreasing flow rate. The very low flow angle at low flow rates causes the flow to circulate often in the numerical inlet section. The result of this is a large drop of tangential velocity in this numerical, non physical, inlet domain, making it unrealistic for low flow rates. This makes the tangential velocity at the inlet boundary needed to give the correct tangential velocity at diffuser inlet very difficult to predict. Because of this it was decided to try different sets of inlet and exit boundary conditions to see if there is another set that does give good results.

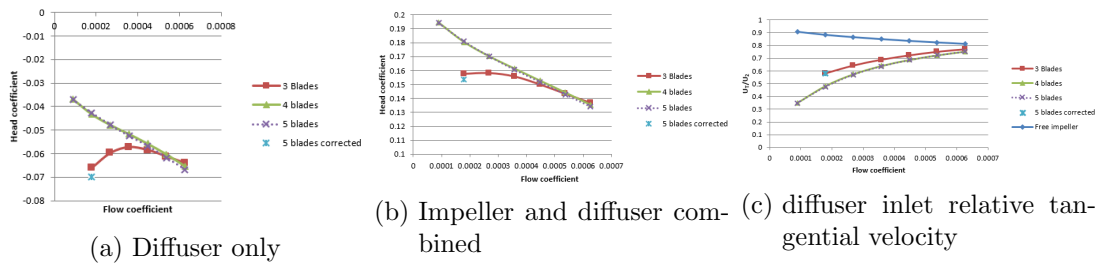


Figure 3.2: Diffuser pressure loss and impeller-diffuser combined head

### 3.2.2 Varying boundary conditions

An attempt was made to find a set of inlet and outlet boundary conditions with good convergence that give good results. Both for the inlet and the outlet a boundary condition must be imposed. First the different boundary conditions are explained, after that the results of combining them shall be discussed.

#### **inlet boundary conditions[15]**

For the inlet boundary conditions, six main types can be identified. Of these six, only three can be used for the current project. The other are for condensable gas flows, harmonic calculations and rotor-stator subprojects. The three types of boundary conditions that can be used are: mass flow imposed conditions, static quantities imposed conditions and total quantities imposed conditions. Each of the main types has a subset of options, based on which quantities are known for the inflow.

**mass flow imposed** has three subsets:

- *meridional flow angle and tangential velocity.* For this subset, the radial and axial velocity relative to the meridional velocity have to be specified, as well as the tangential velocity and the mass flow. This is the boundary condition that was used in the first set of calculations.
- *velocity directions.* For this boundary condition all velocities relative to the absolute velocity have to be specified as well as the mass flow.
- *velocity normal to inlet.* For this subset only the mass flow needs to be specified.

The first and second subset are the same but for different imposed quantities. Since a radial impeller is simulated, the relative radial velocity is 1. Also, the tangential velocity is known, thus the first subset was used. The third subset requires a flow field normal to the inlet and thus cannot be used for diffuser calculations. The downside to this set of boundary conditions is that a constant mass flow is imposed on the inlet boundary condition. Because of this, an inlet section might be needed to get the correct velocity field and mass flow rates at the diffuser inlet radius. If the inlet section is too short, the software predicts large, unrealistic pressure gradients in the region between the diffuser channels. This results in an unrealistic flow field with back flow from the pressure side to the suction side of the diffuser vanes. This was shown in the internship report of Shuja ur Rehman[16] and can be seen in figure 3.3

**static quantities imposed** also has 3 subsets:

- *angle from axial direction.* The magnitude of absolute velocity needs to be imposed, as well as the angle of the velocity with the rotation axis in the radial and tangential plane.
- *angle from meridional direction (static pressure extrapolated).* The magnitude of absolute velocity is imposed, as well as the angle of the radial and tangential velocity with the meridional velocity.

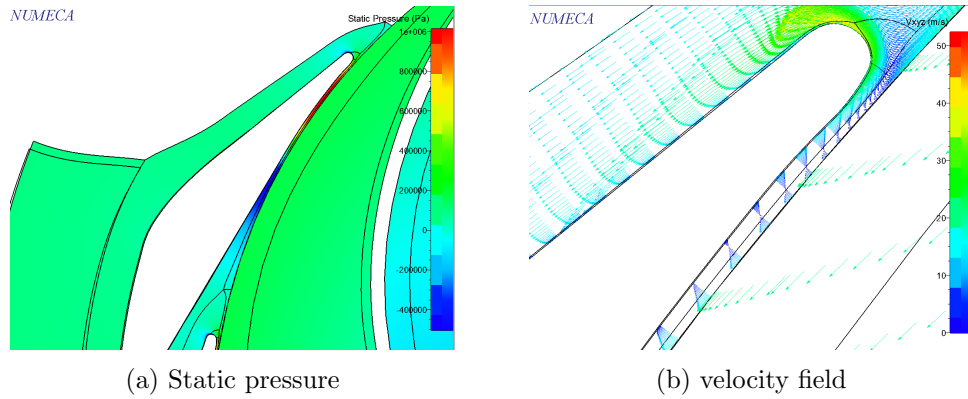


Figure 3.3: figures from[16]

- *velocity components (static pressure extrapolated)*. The radial, tangential and axial velocities need to be imposed.

These are all the same except for the imposed quantities. Since the radial and tangential velocity are known, the last subset could be used as inlet boundary condition. However, since the radial and tangential velocity are imposed, they are assumed constant over the inlet. Thus again a inlet section might be needed to have the correct conditions at the diffuser inlet radius.

**Total quantities imposed** consists of 6 subsets, these are:

- *angle from axial direction( $V$  extrapolated)*. The angle of the radial and tangential velocity with the rotation axis need to be imposed, as well as the absolute total pressure.
- *angle from axial direction( $V_z$  extrapolated)*. The same boundary conditions as the previous subset need to be imposed.
- *velocity direction( $V$  extrapolated)*. The radial, tangential and axial velocities relative to the magnitude of velocity need to be imposed as well as the absolute total pressure.
- *tangential velocity and meridional angle( $V_m$  extrapolated)*. The tangential velocity and the radial and axial velocity relative to the meridional velocity need to be imposed, and again the absolute total pressure
- *flow angle and total conditions in upstream rotational frame ( $V_m$  extrapolated)*. The radial and axial velocities relative to the meridional velocity need to be imposed as well as the angle of the relative tangential velocity with the meridional velocity. Also the relative total pressure and upstream rotational speed are imposed.
- *velocity normal to inlet( $V$  extrapolated)*. The absolute total pressure needs to be imposed.

The first 4 subsets are equal except for the imposed or extrapolated quantities. The fifth subset requires information about the upstream rotor but the result is pretty much the same as for the first four subsets. The last subset again requires a flow field normal to the inlet boundary and thus is useless for diffuser calculations. Since the tangential velocity and meridional angle are known from the impeller calculations, the fourth subset was subjected to a test simulation. Because this inlet boundary condition imposes the pressure at the inlet and calculates the mass flow rate and tangential velocity according, there is no need for a large inlet section. The downside however, is that the dynamic pressure loss over the impeller has to be estimated to get the correct mass flow through the diffuser.

### **outlet boundary conditions[15]**

For the outlet boundary conditions, five main types can be identified. Of these five, two can be used for the current project. The other are for (perfect) gas flows or rotor-stator subprojects. The useful boundary conditions for this project are Pressure imposed and mass flow imposed.

**Pressure imposed** imposes the static pressure at the outlet boundary. there are three methods

- *static pressure imposed.* a uniform static pressure is imposed at the outlet boundary.
- *averaged static pressure.* an averaged value for the static pressure is imposed on the outlet boundary, the pressure profile is extrapolated from the calculations. For this setting, all outlet patches have to be grouped.
- *radial equilibrium.* This boundary condition can only be applied to cylindrical problems with constant radius mesh lines in the circumferential direction. A constant static pressure is imposed in the circumferential direction and the pressure profile from hub to shroud is calculated.

The outflow of the diffuser is non-uniform around the boundary since there are only 4 diffuser channels. So a uniform static pressure is not an appropriate approximation of the physical pressure distribution. Because of this, only the averaged static pressure imposed boundary condition has been given a try.

**mass flow imposed** imposes the mass flow through the outlet boundary. For this method, the related patches, in our case all outlet patches, must be grouped. There are 2 available choices

- *velocity scaling.* The velocity vector is scaled to respect the mass flow rate and the pressure is extrapolated from the results. This is only valid for subsonic flow and isn't recommend when significant backflow is expected.

- *Pressure adaption.* In essence, this boundary condition is equal to the static pressure imposed boundary condition, except the outlet pressure is automatically modified to reach the prescribed mass flow.

Since a static pressure on the outlet boundary isn't an appropriate boundary condition, only the mass flow imposed with velocity scaling option can be used.

### **solid boundary conditions[15]**

Since viscous calculations are performed, the solid boundary conditions are normally also viscous boundary conditions e.g. a no slip boundary condition is prescribed. However, there is an option in Numeca, under expert parameters, to set the solid boundary condition to an Euler solid wall boundary condition. This is done for the last part of the outlet section to reduce friction losses between the end of the physical domain and the end of the larger numerical domain. The numerical domain is chosen larger to give a better approximation of the pressure measured in the discharge pipe. This Euler solid wall boundary condition can also be used in the non-physical part of the inlet domain to reduce friction losses between the numerical inlet boundary and the physical inlet boundary.

### **combinations of boundary conditions**

We found that the mass flow imposed inlet boundary condition leads to large inlet losses, resulting in unpredictable inlet boundary conditions. Or, when no inlet section is applied, doesn't give an appropriate approximation of the pressure field and flow field. The first thing tried to improve the boundary layer selection was to keep the inlet and outlet boundary conditions the same while applying an Euler solid wall boundary condition to the non-physical inlet section of the diffuser. After that, a total quantities imposed inlet boundary condition was applied, with both a mass flow imposed and a pressure imposed boundary condition. The results of these simulations are described in the following section.

### **results of the simulations**

After the initial simulation, for which the mass flow imposed inlet and averaged static pressure imposed outlet boundary condition were used, the first thing tried was imposing the Euler solid wall boundary condition on the inlet section. Although this did lower the hydraulic losses in the inlet section considerably, it still resulted in difficulties predicting the correct inlet boundary conditions. Also this led to the question if, when correct boundary conditions are used, the solution gives a good approximation of the physical flow and pressure fields.

To check if the other boundary conditions could lead to a good approximation, another simulation was run using the total quantities imposed inlet boundary condition, first with a mass flow imposed outlet boundary condition. This led to a difference between the inlet and outlet mass flow of about 0.2 %. However, the mass flow through the

diffuser wasn't constant but showed a slowly diverging periodic pattern, as can be seen in figure 3.4. Thus the pressure imposed outlet boundary condition was imposed instead and another calculation was run. This resulted in approximately the same diverging periodic pattern.

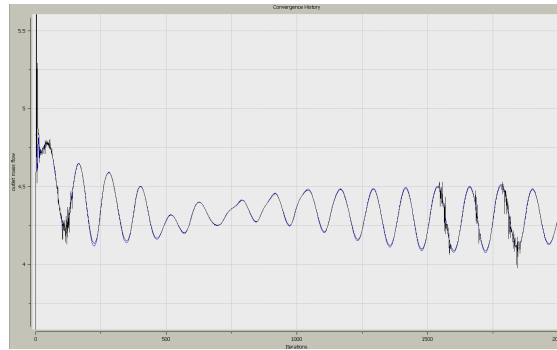


Figure 3.4: inlet and outlet mass flow convergence

Although the second set of boundary conditions doesn't result in a converging solution, the results of the two sets can be compared. This is done by comparing the velocity field at mid plane and the radial and tangential velocity distribution at diffuser inlet. The velocity field for both inlet boundary conditions can be found in figure 3.5. The radial and tangential velocity distribution at diffuser inlet were visualized by creating a cutting plane at the inlet radius. This plane is then selected in the blade to blade view and the radial or tangential velocity is visualized. The radial velocity distribution can be seen in figure 3.6, the tangential velocity in figure 3.7.

When the velocity fields at mid plane are compared, some differences can clearly be seen.

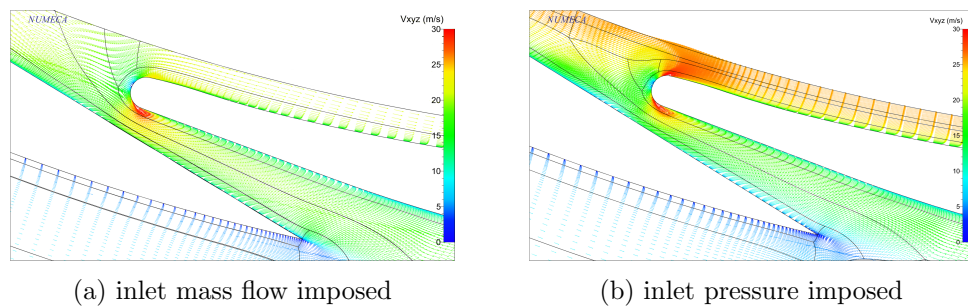


Figure 3.5: velocity field at mid plane

First of all, the magnitude of velocity in the region between the impeller and diffuser vanes, is higher when the inlet pressure is imposed, figure 3.5b, the magnitude of velocity in the channel is larger when the inlet mass flow is imposed. When looking at the area surrounding the vane leading edge, it can be seen that there is region with high velocity on both sides of the vane when the inlet pressure is imposed, and as a result, there is

some backflow into the impeller. When the inlet mass flow is imposed, there is only a high velocity region on the channel side and the flow is directed tangentially near the impeller outlet. The backflow region that was found above can also be seen in the inlet

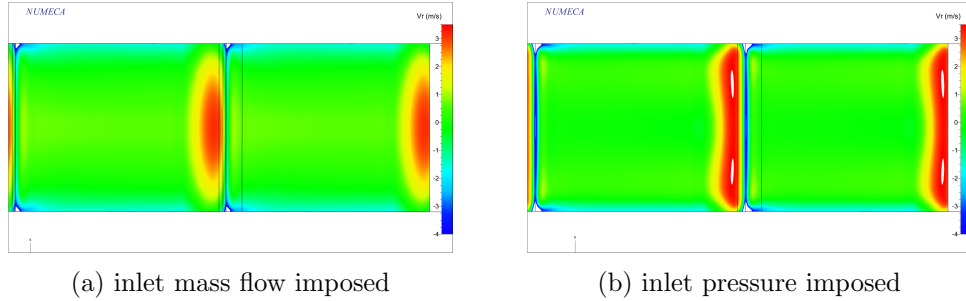


Figure 3.6: Inlet radial velocity distribution

radial velocity distribution. Two consecutive blades are shown, so the vane leading edge is approximately in the center of the image. For the pressure imposed inlet boundary, figure 3.6, we can clearly see a dark blue area, corresponding to negative radial velocity, where the mass flow imposed inlet boundary shows a greenish area, corresponding to approximately zero radial velocity. Also when the mass flow is imposed, a local maximum is found upstream of the leading edge, in the center of the diffuser width, whereas two local maxima are found, at approximately  $\frac{1}{4}$  and  $\frac{3}{4}$  of the diffuser width when the pressure is imposed. A possible explanation is that the hub and shroud boundary layers are fully developed when the mass flow is imposed, because there is a long inlet section. When the pressure is imposed there is almost no inlet section so the boundary layer is much smaller.

Lastly, when looking at the tangential velocity, again there is a clear difference. When

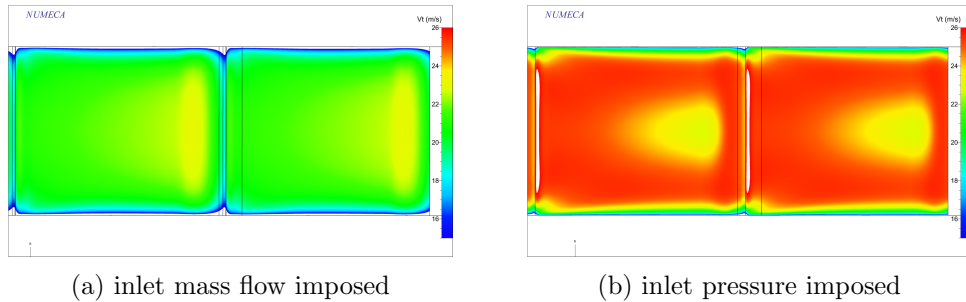


Figure 3.7: inlet tangential velocity distribution

the pressure is imposed at the inlet, there is a maximum just downstream of the leading edge and a local minimum just upstream of the diffuser channel. When the mass flow is imposed, there is a minimum just downstream of the leading edge and a maximum just upstream of the diffuser channel.

### 3.2.3 conclusion

Based on the simulations that were run it was concluded that the set of boundary conditions that has a converging solution suffers from too large losses in the non-physical inlet domain. This results in unpredictable inlet boundary conditions and probably an incorrect approximation of the physical flow field. However, the set of inlet boundary conditions that does show promising results suffers from a diverging solution. So the method of free diffuser calculations in this case isn't able to give a good approximation of the physical flow field.

## 3.3 Nonlinear hydraulic calculations

Since a good approximation of the flow field using free diffuser calculations couldn't be found, the decision was made to switch to nonlinear hydraulic calculations. The idea behind this method is that a time averaged steady state flow can be found around which flow perturbations exist that make it unsteady. These perturbations are Fourier decomposed in time and transport equations are obtained for each time frequency. Alongside solving the time averaged steady state flow, there are two extra sets of conservation equations per frequency which need to be solved. Inserting the deterministic stresses into the time averaged flow solver makes the method nonlinear[15].

To be able to do nonlinear hydraulic calculations a model of the complete pump, from impeller inlet to diffuser outlet, is needed. It was decided to use the model of a 35Y2 impeller, which Niels Platenkamp had used before to test the result of varying the number of diffuser vanes. This model includes front and back leakage paths as well as balancing holes. The diffuser model with 4 vanes was modified with a groove, of which the depth and relative distance from the trailing edge were varied. Although this model pump in itself is not a low flow high head pump, the results can be correlated to the test results of the grooved diffuser tested in the low flow high head project. The model was chosen because it was readily available and showed good convergence in earlier numerical computations.

### 3.3.1 diffuser model

It was decided to test the effect of groove depth and relative position so a model is needed in which these values can be adjusted. To be able to do this a solid model of  $\frac{1}{4}$  of the diffuser is created using PTC's pro/Engineer. Of this model the point coordinates and wire-frame are exported to an igs file, which was then loaded into NUMECA IGG. Next, blocks were placed manually in the wet parts of the diffuser, such that their vertices were mapped on the wire-frame of the Pro/E model. This results in a model with unstructured nodes, e.g. the nodes on hub and shroud aren't aligned. As can be seen in figure 3.8. The next step was to move the block vertices to create a nicely structured topology. This was done using a python script, the result can be seen in figure 3.9. The final step then was to specify the number of grid points for the blocks, and the grid clustering, uniform in the inlet and outlet section, clustered to one or both ends when

solid walls are present. A hyperbolic tangent clustering was specified for the width of the diffuser, with a starting cell width of 0.02 mm. This results in a structured mesh, ready to be coupled to the impeller. All the steps done with IGG were captured and saved to a python script, such that when the groove position or depth is changed, block and mesh generation is handled by the python script.

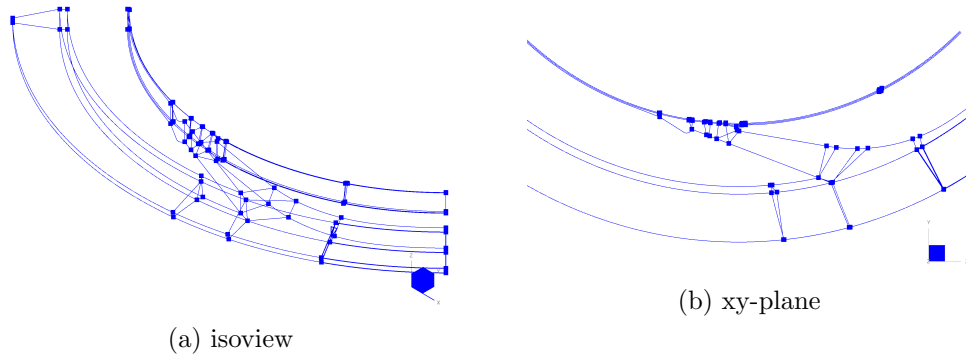


Figure 3.8: unstructured block grid

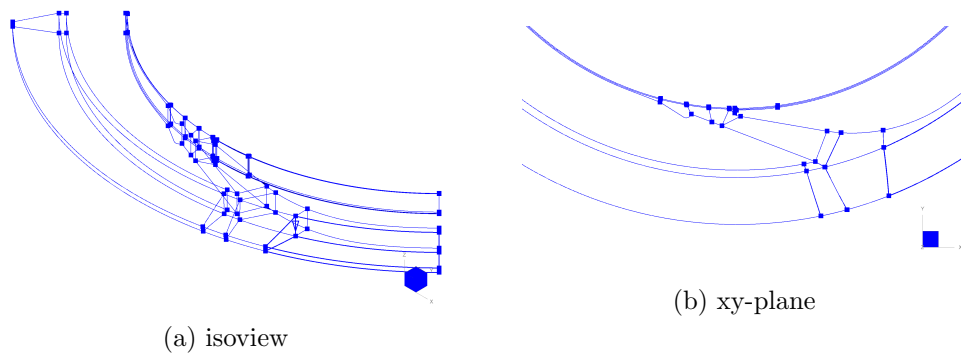


Figure 3.9: structured block grid

### 3.3.2 FINE/Turbo settings

Now that the model and computational grid are complete, the next step is to set up FINE/Turbo. Before setting up and starting the nonlinear hydraulic calculations, an approximate initial solution is calculated. This saves computation time and improves convergence. When the groove depth or position is changed, the previous solution can be used as initial solution. All calculations are run for the design flow rate, results are plotted against groove depth and groove position.

### creating an initial solution

To create the first approximate initial solution a steady computation is used, with Turbulent Navier-Stokes mathematical model and Spalart-Allmaras turbulence modeling. On the inlet boundary a mass flow of  $13.89 \text{ kg s}^{-1}$  is imposed and on the outlet boundary a averaged static pressure of  $1\,501\,300 \text{ Pa}$ . For the Numerical model, the coarsest  $2\,2\,2$  grid is specified for the initial run, and thus only 1 grid level. After the calculation is done, a new computation is set up, now for the  $1\,1\,1$  grid. Number of grid levels is changed to 2 and coarse grid initialization is disabled. The solution of the first calculation is used as initial solution. Both computations were run through 10.000 iterations, taking in total some 6 hours to complete. After this the nonlinear hydraulic computation was setup. The NUMECA basic harmonic configuration was used, with 3 frequencies per perturbation and 1 perturbation per blade row, the characteristic velocity was set to  $60\,000 \text{ m s}^{-1}$  to ensure stability. The numerical model is set to the  $0\,0\,0$  grid level, without coarse grid initialization. The solution of the previous steady calculation is imposed as initial solution.

### 3.3.3 results

To compare the results of the different grooves the results need to be post processed. To be able to do this, first the time dependent solution has to be rebuild. Using the Harmo2Time module of Fine/Turbo, the flow can be reconstructed in the time domain. 90 timesteps are selected, to give a rotor rotation of  $1^\circ$  per timestep. Then CFview starts to calculate the solution for every time step, after which the solution is loaded into CFview. Using a python script, the static and dynamic pressure are extracted at the pump inlet, rotor-stator interface and pump outlet to examine the impeller and diffuser generated head in time as well as the overall head in time. The same shall be done for 1 impeller and diffuser passage. Also, the dynamic and static pressure and the radial and tangential velocity are extracted at inlet and outlet to 1 diffuser channel. This way the effect of blade passing can be examined. This can also give insight into the effect of the groove on the flow field and pump performance. The acquired results are further post processed using Excel. For visualization of the flow field, images are made of the static pressure and magnitude of velocity for the complete pump, and of the velocity field for a close up of 1 diffuser channel. This is done for every time step. The head generated by the pump with different groove positions can be calculated by subtracting the total pressure at the inlet from the total pressure at the outlet. The impeller generated head by subtracting the total pressure at inlet from the total pressure at the RS interface, and the diffuser head loss by subtracting the total pressure at the RS interface from the total pressure at the exit of the diffuser. These can then be compared for the different groove positions to show the effect of the groove position on generated head. The same can be done for the single channel results. Since a single channel is considered, the effect of the groove and of the blade passing the diffuser leading edge becomes more prominent. The head generated by the pump over time can be seen in figure 3.10 for 90 time steps, equal to one quarter of a rotation of the impeller.

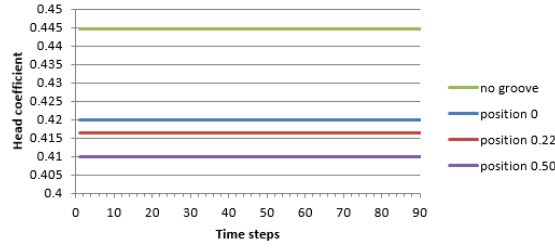


Figure 3.10: Pump head coefficient vs time steps

The head is constant in time, which was also found for the other examined quantities. Because of this, for all quantities, the difference is given as a percentage of the initial(ungrooved) situation. An example calculation for the head can be seen in equation (3.1).

$$H_{change} = \frac{H_{grooved} - H_{ungrooved}}{H_{ungrooved}} \quad (3.1)$$

If we then first look at the characteristics for the complete pump, figure (3.11), we see that the total head and static head both decrease with the addition of a groove to the diffuser. Also, it can be seen that the generated total and static head decrease

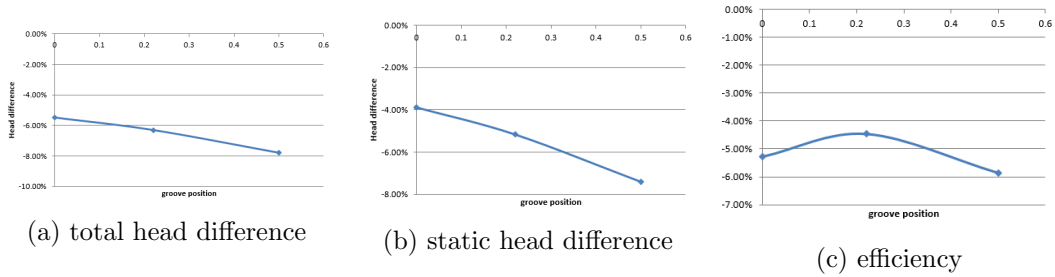
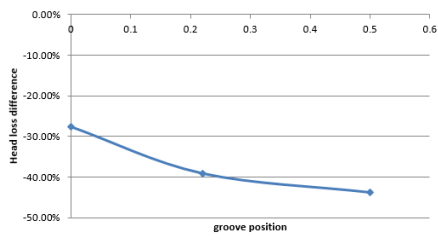
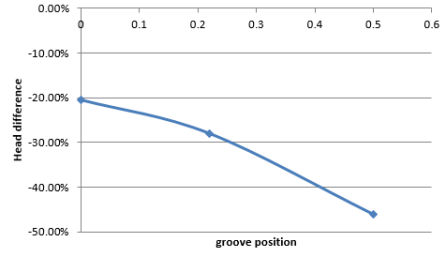


Figure 3.11: complete pump characteristics

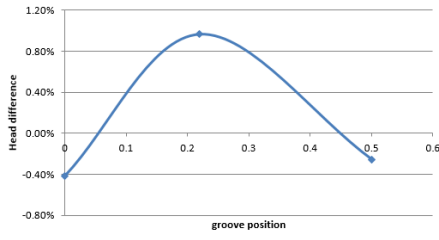
with increasing distance of the groove to the diffuser channel. If we look at the pump efficiency however, we see that this doesn't decrease in the same way as the head. This is a result of the required torque decreasing with increasing distance of the groove to the diffuser channel. Looking at the impeller and diffuser separately, figure 3.12, we see that the total head loss and static head rise over the diffuser show good comparison with the complete pump characteristics. The impeller total and static head rise however are quite different. They show a decrease when the groove is placed right at the start of the diffuser channel. However, they increase with increasing groove distance. Up until a certain distance after which they both decrease again. From this it can be concluded that adding a groove to the diffuser has a negative effect on the pump characteristics when looking at the design flow rate. However, since we only simulated for one flow rate, we cannot say much about the effectiveness of the groove, or the effect of its position for



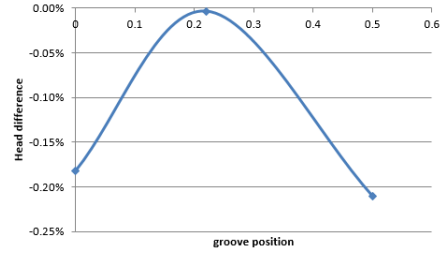
(a) diffuser total head difference



(b) diffuser static head difference



(c) impeller total head difference



(d) impeller static head difference

Figure 3.12: Diffuser and impeller characteristics

off-design flow rates. More simulations, at different flow rates have to be done. However, time didn't allow this.

## 4 testing

In this final part of the report, the physical testing shall be discussed. Due to some unexpected long delivery times, only 5 diffusers were tested before the end of my internship, and only 1 test was run with all the pressure gauges. Tests were run with a standard diffuser, a diffuser with a shallow groove, a diffuser with a deep groove, a grooved round diffuser and a slotted diffuser. CAD images of these concepts can be seen in figure 4.1. Because the diffuser with the shallow and deep groove look similar, only the shallow grooved diffuser is shown. The choice for these 5 diffusers to be tested first was made based on the expected results.

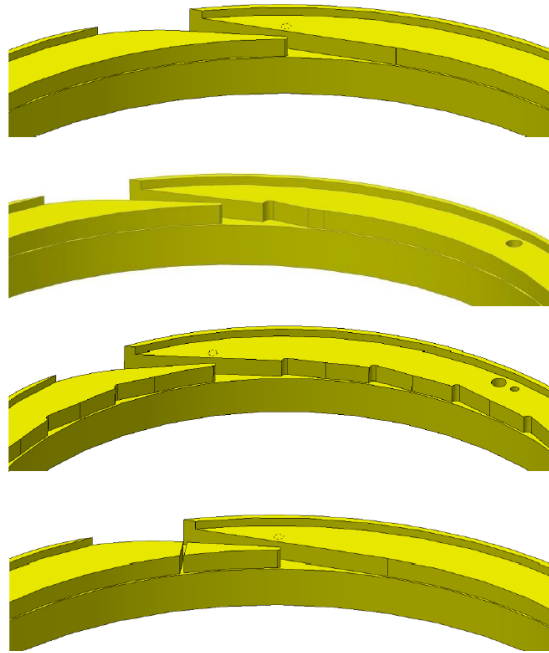
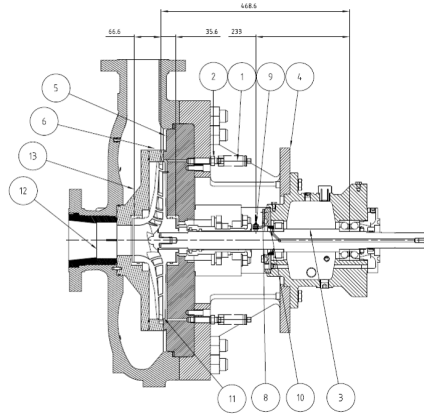


Figure 4.1: CAD images of the tested diffusers, from top to bottom: standard, grooved, grooved round and slotted

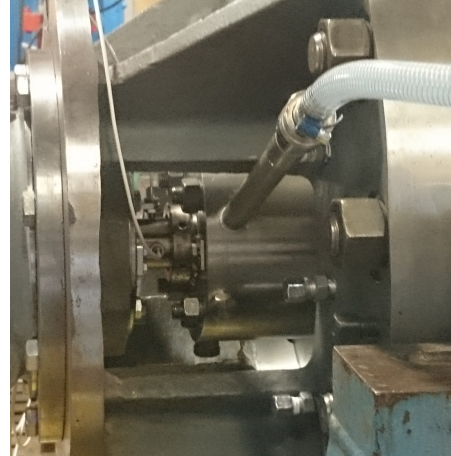
When the pressure gauges were fitted, also the standard diffuser was fitted to the pump again, to create a base to which the other results can be compared. Since there wasn't any time left to test other diffusers with pressure around the impeller, the pressure data won't be displayed in this report.

## 4.1 test stand

for the physical tests a test pump has been built, which is shown schematically in figure 4.2a. This consists of a standard pump housing to which a composite diffuser (6,13) and modified back pull out unit was fitted. Also an insert (12) is fitted in the inlet pipe such that the diameter of the inlet is the same as the impeller inlet diameter.



(a) schematic



(b) close up of the bearing bracket

Figure 4.2: test pump

The back pull out unit was fitted with the 40c impeller (11) which has also been modeled for the free impeller calculations. Further it consisted of the pump casing back plate (5), in which holes were made for the pressure gauges, a bearing bracket (4), to which proximeters (8,9) are fitted, and pipe stubs (2) for the pressure gauges (1). Finally it featured a shaft (3) fitted with strain gauges and an antenna to acquire the data. When we look at the close up of the bearing bracket we can see the 2 proximeters, with white data cables. Also the seal feed and the pipe stubs to which the pressure gauges shall be fitted can be seen.

## 4.2 test results

The results of the different diffusers on the pump head at shut off, BEP and several flow rates are shown in figure 4.3. The resulting relative efficiency is shown in the same figure. At BEP it is seen that adding a groove or a slot lowers the head generated by the pump, just as was predicted by CFD. However, for the grooved diffusers it can be seen that the Q-H curve shows a translation of the complete curve towards lower flow rates, so this has no effect on stability. The grooved round and slotted diffuser show some improvement in stability of the curve, however this is not enough to be called significant. Also the efficiency of all alternative diffusers is lower than that of the standard diffuser.

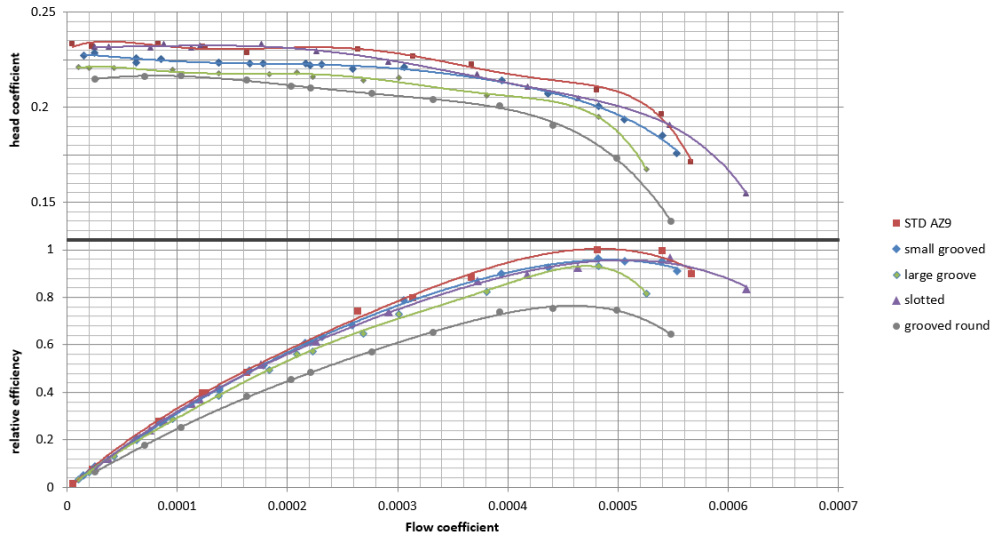


Figure 4.3: head coefficient - flow coefficient and relative efficiency - flow coefficient curves for the tested designs

### shaft displacement

Measured shaft displacement is shown in figure 4.4. The 0 position is the measured displacement when the pump is turned off.

It can be seen that the shaft positions itself upwards when the pump is running. Also a nearly circular movement pattern can be seen with small variations around this circle. Influence of the operating point on this circle is minimal, as can be seen in figure 4.4. The spread of the measurements did seem to increase towards shutoff. Also the diameter of the circle became smaller for lower pump speeds.

### conclusion

Changing diffusers didn't have a significant result on the shut off head and head rise to shut off. Also the effect of the different diffusers on measured shaft displacement was minimal. The measured data do give rise to some questions about rotor-dynamics of the system and the Lomakin-stiffness in relation to the radial induced forces in the pump. If the effects of all forces in the pump can be quantified and calculated, other diffuser designs, with 2 or 1 channel, could also become mechanically possible. Further research is thus needed.

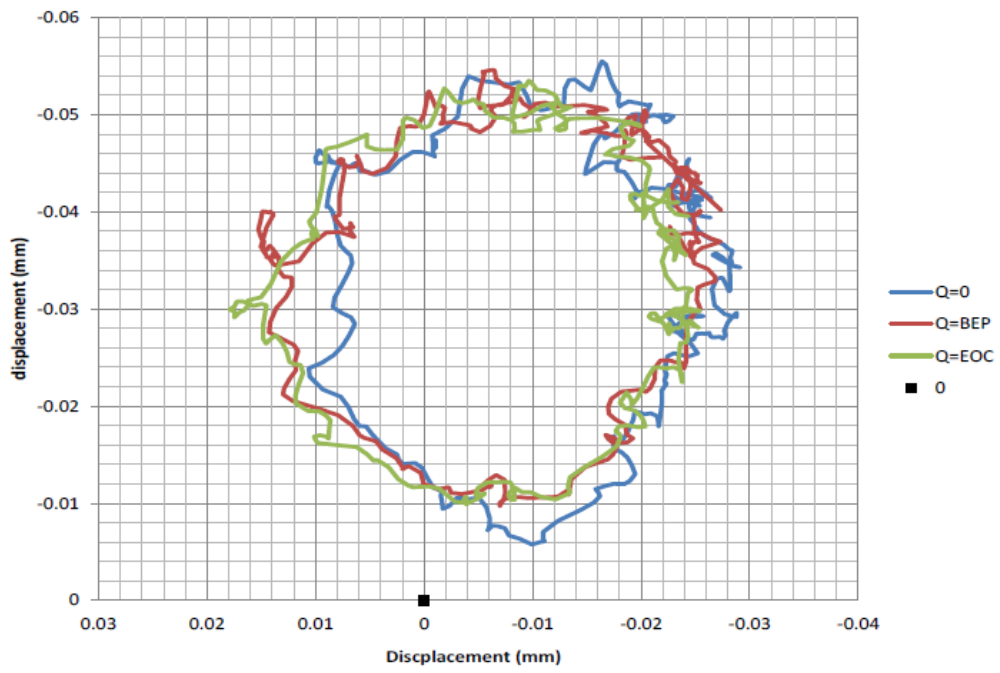


Figure 4.4: Measured shaft displacement

# Bibliography

- [1] Flowserve <http://www.flowserve.com/About-Flowserve/Corporate-Information/Flowserve-At-a-Glance>, December 2014
- [2] Gülich J.F. *Centrifugal pumps*. second edition, Springer, Berlin, 2010.
- [3] Atif A, Benmansour S, Bois G, et al. *Numerical and experimental comparison of the vaned diffuser interaction inside the impeller velocity field of a centrifugal pump*. Science China Technological Science, (2011), volume 54
- [4] Gaetani P, Boccazzi A, Sala R. *Flow field in the vaned diffuser of a centrifugal pump at different vane setting angles*. Journal of fluids engineering, (2012) volume 134
- [5] Ohta Y, Takehara N, Okutsu Y, Outa E. *Effects of diffuser vane geometry on interaction noise generated from a centrifugal compressor*. Journal of thermal science, (2005), volume 14, No.4
- [6] Ohta Y, Okutsu Y, Goto T, Outa E. *Aerodynamic performance and noise characteristics of a centrifugal compressor with modified vaned diffusers*. Journal of thermal science, (2006), volume 15, No.4
- [7] Ohta Y, Goto T, Outa E. *Effects of tapered diffuser vane on the flow field and noise of a centrifugal compressor*. Journal of thermal science, (2007), volume 16, No.4
- [8] Goto T, Ohmoto E, Ohta Y, Outa E. *Noise reduction and surge margin improvement using tapered diffuser vane in a centrifugal compressor*. Journal of thermal science, (2010) volume 19, No.1
- [9] Ohta Y, Fujisawa N. *Unsteady behavior and control of vortices in centrifugal compressor*. Journal of thermal science, (2014), volume 23, No.5
- [10] Sakaguchi D, Fuji T, Ueki H, Ishida M, Hayami H. *Control of secondary flow in a low solidity circular cascade diffuser*. Journal of thermal Science, (2012) Volume 21, No.4
- [11] Sutardi, Ching C.Y. *Effect of different sized transverse square grooves on a turbulent boundary layer*. Experiments in fluids, (2003), Volume 34
- [12] Sutardi, Ching C.Y. *The response of a turbulent boundary layer to different shed transverse grooves*. Experiments in fluids, (2003), Volume 35

- [13] Kurokawa J, Saha S, Matsui J, Kitahora T. *Passive control of rotating stall in a parallel-wall vaneless diffuser by radial grooves*. Journal of fluids engineering, (200), Volume 122
- [14] Saha S, Kurokawa J, Matsui J, Imamura H. *Passive control of rotating stall in a parallel-wall vaned diffuser by J-grooves* . Journal of fluids engineering, (2001), Volume 123
- [15] NUMECA International. *Usermanual Fine/Turbo*. Version 9.0 A, Numeca, Brussels, april 2013.
- [16] Shuja ur Rehman. *Internship assignment Flowserve Hengelo*. Hengelo, November 2012.